ChemCatChem

Research Article
doi.org/10.1002/cctc.202401586

Chemistry Europe
European Chemical Societies Publishing

www.chemcatchem.org

Cu-Based Catalysts for the One-Pot Condensation–Hydrogenation of Cyclopentanone to Produce Valuable SAF Precursors

Nicola Schiaroli,*[a, b] Lorenzo Scaglione,[a, b] Riccardo Mandioni,[a] Francesca Foschi,[a] Sandro Recchia,[a] and Carlo Lucarelli*[a, b]

A process combining aldol condensation and hydrogenation of bio-based cyclopentanone (CPO) in a one-pot reaction is proposed. Cu-based bifunctional catalysts obtained from hydrotalcite-type precursors were found highly active in mild reaction conditions (i.e., 130–170 °C), producing valuable bicyclic (C10) and tricyclic (C15) aliphatic alcohols/ketones with interesting application as sustainable aviation fuel (SAF) precursors with enhanced properties. The presence of surficial strong basic sites active in aldol condensation, together with the formation of highly dispersed copper nanoparticles able to catalyze C=C and C=O hydrogenation (TOF of 0.06–0.16 s^{-1}), assured high catalytic efficiency and fine control of the products nature and distribution. From the optimization of both catalysts formulation and reaction conditions it was found that, properly tuning the Cu content, it is possible to drive products distribution towards the production of bicyclic (C10) aliphatic alcohol with high selectivity (75% at total CPO conversion, when Cu = 10 wt %, at 170 °C, 1.0 MPa of H_2) and short reaction time (4 h). The optimized catalyst formulation showed impressive stability over multiple reaction/regeneration cycles, demonstrating the high potential of the proposed catalytic process for future applications in sustainable biofuels production.

1. Introduction

The production of high-quality transportation fuels from renewable sources is a promising route to reach the carbon neutrality goal of the heavy transportation sector, which is generally not suitable for electrification. In this context, the production of first-generation biofuels such as bioethanol[1] (from fermentation processes) and hydrotreated vegetable oil[2] (HVO) obtained from edible energy crops, represents an already consolidated market on a global level, which partly replaces that of petrol and diesel fuels obtained from traditional fossil resources. On the other hand, the environmental and ethical problems linked to the intensive exploitation of edible resources pose the need to direct the production of biofuels towards the use of second-generation feedstocks such as lignocellulosic biomass and organic waste. Starting from these highly available resources, second generation biofuels can be produced though Fischer Tropsch (Biomass to liquid, BtL)[3] using synthesis gas produced from biogas[4–7] or biomass gasification,[8] from ethanol derived from lignocellulosic waste,[9] or from bio-oils produced through pyrolysis.[10] Aviation fuel market represent one of the most hard-to-abate sectors as it is hardly consistent with the use of green hydrogen or electricity in the foreseeable future.[11,12] Conventional aviation fuel is composed of molecules of approximately 7 to 18 carbons (average of 12C atoms) divided between linear and branched alkanes, aromatics, and cyclic hydrocarbons. The latter comprise a diverse spectrum of molecules which are generally associated with high-energy densities and are capable of potentially replace the aromatic content typical of oil-based fuels, main responsible for particulate emissions and sooting.[13] In this context, the production of new sustainable aviation fuels (SAF) formulations is driving particular attention. Among different synthetic strategies, aldol condensation of bio-based ketones obtainable from lignocellulosic biomass,[14,15] represent an elegant synthetic strategy to elongate carbon chains while decreasing the oxygen content of the product mixture at mild reaction conditions.[16] The aldol condensation of cyclopentanone (CPO, obtainable from bio-based furfural[17,18]) to the mono-condensed (2-cyclopentylidene-cyclopentanone, C10) and di-condensed product (2,5-dicyclopentylidene-cyclopentanone, C15) has the potential to produce highly valuable precursors for the production of SAF with improved properties. The reaction has been carried out over basic metal oxides such as MgO, CaO-CeO_2, Li-Al, and Mg-Al hydrotalcites at 150 °C (reaction time of 8 h)[19] and while the hydrophobization of MgO improves the performance of the solid oxide in the reaction,[20] MgO-ZrO_2 rich in surficial basic

[a] Dr. N. Schiaroli, Dr. L. Scaglione, Dr. R. Mandioni, Dr. F. Foschi, Prof. S. Recchia, Prof. C. Lucarelli
Dipartimento di Scienza e Alta Tecnologia, Università degli Studi dell'Insubria, Via Valleggio 9, Como 22100, Italy
E-mail: nicola.schiaroli@uninsubria.it
carlo.lucarelli@uninsubria.it

[b] Dr. N. Schiaroli, Dr. L. Scaglione, Prof. C. Lucarelli
Consorzio INSTM, Research Unit of Como, Via Giuseppe Giusti 9, Firenze50121, Italy

Supporting information for this article is available on the WWW under https://doi.org/10.1002/10.1002/cctc.202401586

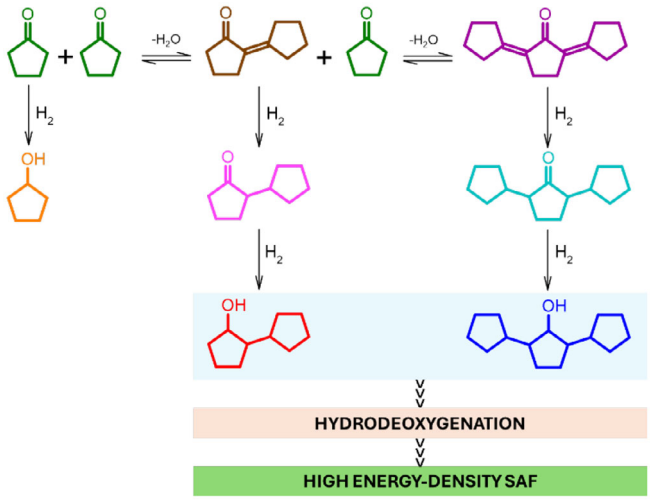

Scheme 1. Main reactions involved in the proposed one-pot aldol condensation–hydrogenation process for the production of valuable SAF precursors.

sites, displayed high yield of C10 (86%) at 130 °C after 4.5 h of reaction.[21] Different Mg-Al mixed oxides were found active in the reaction obtaining C10–C15 compounds in different yields depending on Mg/Al molar ratio and process temperature[22] while Deng et al.[23] performed the self-condensation of CPO over MOF-encapsulating phosphotungstic acid catalysts reaching high selectivity towards C10 production (>95% at 130 °C) but a low CPO conversion (≈ 45%). Although all these different catalyst formulations are considerably active in the reaction, aldol condensation suffers from a lack of control in terms of C10 selectivity, due to easy further reaction of this latter with the monocyclic ketone to form heavier compounds (C15–20) which despite exhibiting a higher energy density, if produced in high amounts can considerably increase mixture freezing point affecting its final applicability in common flights engines. In a recent work, Wang et al.[24] proposed a two-step process in which homogenously catalyzed CPO aldol condensation is followed by an hydrodeoxygenation process (Pd/C and HZSM-5, 200 °C, 12 h, 6 MPa of H_2) to form bicyclic and tricyclic alkanes, evidencing how an optimal control of condensation step is crucial to obtain a mixture with high-energy density products compatible with SAF formulations. A selectivity towards C10 of 69%–75% and C15 of 25%–31% were found to be an optimum compromise between density and freezing point of the obtained fuel mixture. With the aim to integrate CPO aldol condensation and hydrodeoxygenation processes in a one-pot reaction, Deng et al.[25] developed a bifunctional catalyst composed by Pd encapsulating into ZSM-5 mesoporous zeolite, obtaining high catalytic efficiency in bicyclic alkane synthesis in mild reaction conditions (160 °C, 1 MPa of H_2, 12 h) but almost completely suppressing the production of C15 compounds in the tested conditions. Remarkably, Li and coworkers,[26] found that Cu/Al_2O_3 is an active catalyst in the CPO condensation–hydrodeoxygenation process at high temperature (280 °C, 1 MPa of H_2, 6–8 h) both in liquid and in gas phase, achieving total CPO conversion in different reaction conditions but hardly controlling the selectivity of the reaction towards C15–20 hydrocarbons (40% in the liquid phase and 35% in the gas phase.). Starting from these premises, the present work investigates the use of bifunctional Cu/Mg/Al/O catalysts in the one-pot CPO aldol condensation–hydrogenation process, with the aim to produce high-energy density C10–15 mixtures rich in valuable C10 SAF precursors (Scheme 1) by optimizing both catalyst formulation and reaction parameters under mild reaction conditions.

According to our best knowledge, studies regarding the application of such Cu/Mg/Al/O catalysts in the proposed integrated process have not previously been reported in scientific literature. From the optimal combination of highly active Cu^0 sites, able to activate H_2, and dispersed basic sites active in aldol condensation reaction, it is possible to achieve high catalytic efficiency in the combined process, together with a fine control of its selectivity towards the controlled formation of both low freezing point C10 precursors and higher energy density C15 tricyclic alcohols.

2. Results and Discussion

2.1. Aldol Condensation Over (Cu)Mg/Al/O Catalysts

The XRD patterns of the catalysts before calcination (Figure 1a) show the formation of the hydrotalcite-type precursors (HT) in agreement with the insertion of Cu^{2+} cations into the brucite-type layer, favored by the presence of Mg^{2+}.[27] After calcination, the XRD analyses (Figure 1b) confirmed the decomposition of the precursors towards the formation of an oxidic matrix with poor crystallinity and a specific surface area comprised between 175 and 211 m^2/g. The Cu-based catalysts are composed by a MgO phase in which Cu^{2+} is incorporating, and a spinel-like structure consisting of Cu/Mg/Al/O mixed oxide. The peaks shape and position were not affected by Cu^{2+} concentration, and the formation of a significant amount of CuO or Cu_2O phase was not observed. Although their minimal formation could not be excluded,[28] this seems to further confirm the prevalent inclusion of Cu^{2+} ions within the oxide matrix. To understand how the operative conditions influence the aldol condensation of CPO, preliminary catalytic tests were performed over the Cu-free sample (MgAl4). The catalytic activity as a function of reaction temperature is depicted in Figure 2a, where the products distribution is expressed in terms of dimer and trimer yields. The conversion of CPO rises at increasing temperature, hitting a value of 98% at 150 and 170 °C. The detected products, regardless of reaction conditions, are the α, β-unsaturated cyclic ketones 2-cyclopentylidene-cyclopentanone and 2,5-dicyclopentylidene-cyclopentanone, named C10 and C15, respectively. It is noteworthy that the sum of the products yields corresponds to the reactant conversion for all the reactivity tests, meaning that no carbon losses were detected. The distribution of the condensation products is greatly influenced by the temperature of the process. At 130 °C most of the CPO is converted to C10 which hardly undergoes further condensation, giving a poor C15 yield of 14%. From 150 °C it is possible to observe a reversal of the

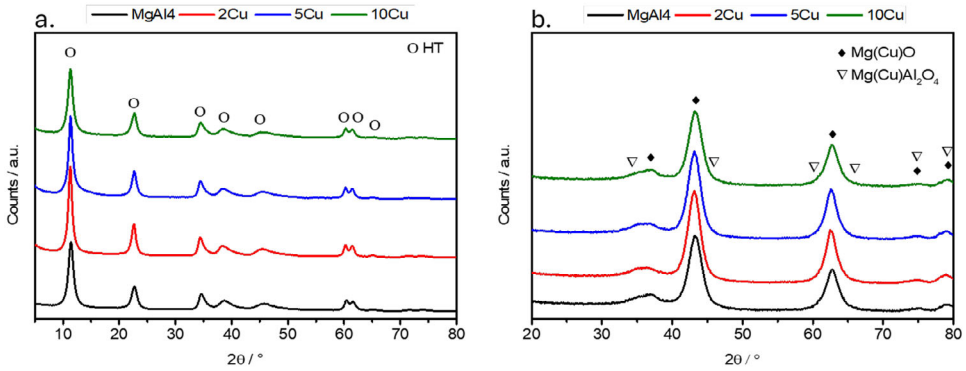

Figure 1. XRD patterns of the catalysts: a) before calcination and b) after calcination at 600 °C for 6 h.

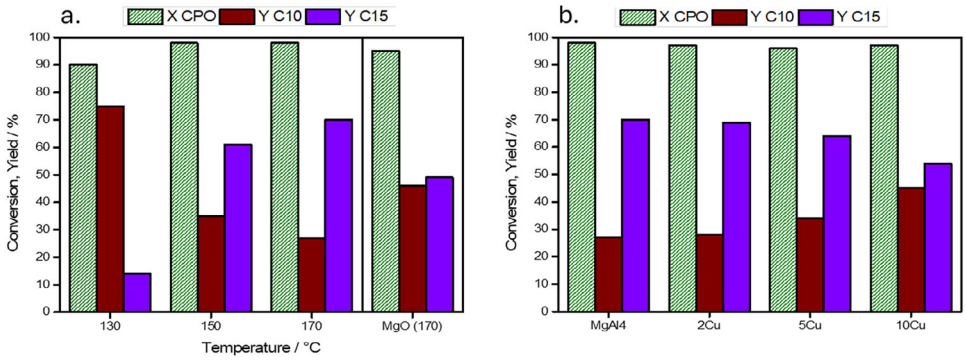

Figure 2. a) MgAl4 and MgO catalytic activity as a function of reaction temperature and b) Catalysts performance at 170 °C as a function of the Cu content. Reaction conditions: 44 mmol of CPO, 0.5 g of CAT and 30 mL of cyclohexane, reaction time of 4 h, N_2 pressure of 1.0 MPa.

products distribution, C15 is formed with a yield of 61% which increases to 70% at 170 °C. The activity of MgAl4 catalyst, composed of MgO and Mg/Al/O mixed phases, is higher than that of pristine MgO (at 170 °C) synthesized and calcined using the same methodology (SS_{BET} of 130 m^2/g) which attained almost equal C10 and C15 yield of 46% and 49%, respectively. The influence of Cu on the catalyst activity in aldol condensation at 170 °C is shown in Figure 2b. Although a basically constant CPO conversion was obtained, at increasing Cu concentration (2, 5 or 10 wt %), a slight inhibition of aldol condensation reaction can be observed.

In accordance with its low Cu content (2 wt %), 2Cu, and MgAl4 catalysts show similar activity while 5Cu and 10Cu catalysts exhibited, in line with the increased Cu concentration (5 and 10 wt %), substantially lower yields in terms of C15 product, revealing a less reactive catalytic system in condensation reaction.

The calcined samples were characterized by a comparable specific surface areas and similar adsorption and desorption type V isotherms, typical of mesoporous materials (Figure S1) as confirmed by the pore size distribution of the different samples (Figure 3a), which revealed an average dimension in the range of 9–17 nm, where the presence of Cu seems to slightly decrease the average pore size.

The surface basicity of the catalysts was evaluated by means of CO_2-TPD analyses that showed similar CO_2 desorption peaks with asymmetrical shape (Figure 3b). From the deconvolution of the profiles, it is possible to identify three main desorption peaks attributable to weak (50–150 °C), medium (150–250 °C), and strong (>250 °C) basic sites likely related to the presence of Brønsted OH, Lewis Mg—O and O^{2-} surface sites respectively.[29] Regardless of Cu content, the catalysts are characterized by the presence of mainly strong basic sites, which account for roughly half of the total, and only a small amount of weak Brønsted sites. Although establishing a clear correlation between these distributions and the catalysts activity is not straightforward; by normalizing the amount of CO_2 desorbed (and therefore the total of basic sites) on the different specific surface areas, it is possible to notice how this value (expressed as μmol CO_2/m^2) decreases with increasing Cu content. These results are in line with the catalytic activity registered with the 5Cu and 10Cu samples, whose lower tendency to form C15 product is likely related the lower concentration of dispersed MgO, which leads to a reduced density of surface basic sites.

2.2. One-Pot Condensation–Hydrogenation of CPO

The Cu-based catalysts were tested in the condensation–hydrogenation process by carrying out the reactions in a H_2 atmosphere (1.0 MPa). The behavior of the samples in reducing conditions was studied by means of H_2-TPR analyses (Figure 4).

The obtained profiles show different $Cu^{2+} \rightarrow Cu^0$ reduction temperatures for the three catalysts. The increase of the Cu

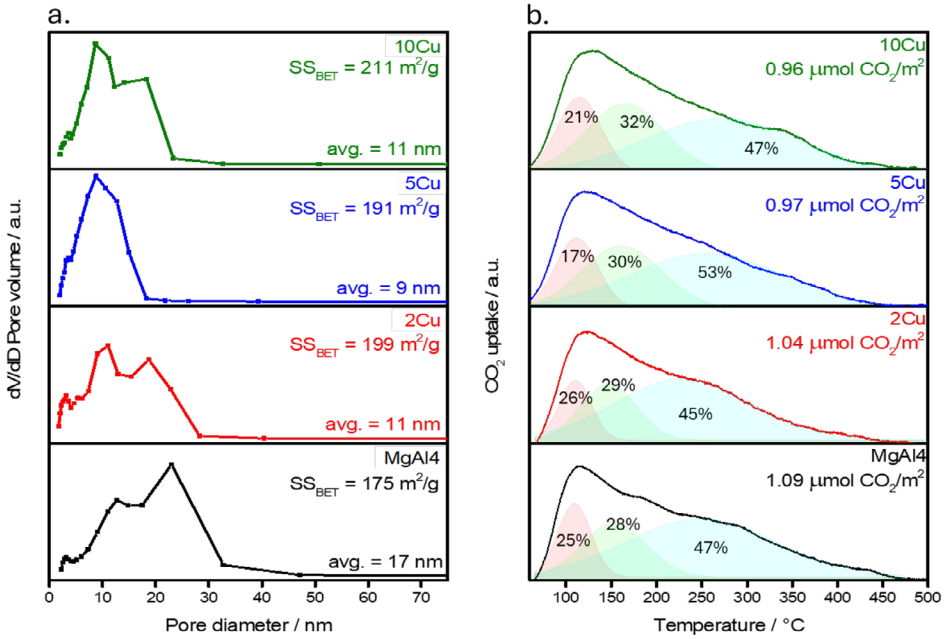

Figure 3. a) Pore size distributions of the catalysts after calcination and b) CO_2-TPD profiles of the catalysts after reduction. The percentages expressed within the curves refer to the distribution of weak (50–150 °C), medium (150–250 °C) and strong (>250 °C) surficial basic sites.

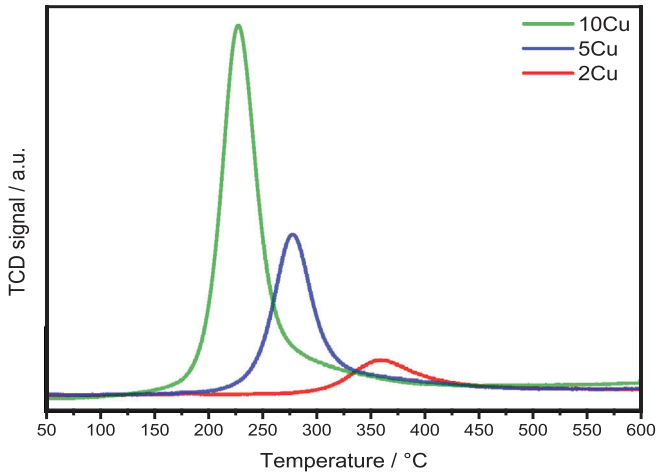

Figure 4. H_2-TPR profiles of the calcined Cu-based catalysts.

content gives rise to a shift of the Cu^{2+} reduction towards lower temperatures together with an increase of the TCD signal intensity in accordance with catalysts composition. The H_2-TPR profiles show asymmetric peaks due to the overlapping of the reduction of different Cu^{2+}-containing species interacting with the oxide phases.[30] In particular, the profile of 10Cu catalyst shows a reduction peak with a maximum at 228 °C which is associated with highly active surficial Cu-containing species with low interaction with the support (metal-support-interaction, MSI) while the broader peak tail (T > 250 °C) is likely related to the presence of hard to reduce species such as $Cu(Mg)Al_2O_4$ or $CuAl_2O_4$.[31] The reduction peak of 2Cu catalyst is centered to a sensibly higher temperature of 358 °C which is related, in accordance with other works,[32,33] to the activation of highly dispersed Cu particles with stronger MSI.

The products obtained in the condensation–hydrogenation process are shown in Figure 5a. Differently from what observed in the previous catalytic tests, the final mixture is not composed of α, β-unsaturated cyclic ketones, but instead shows the presence of C10–C15 molecules that, depending on reaction conditions, consist of aliphatic cyclic ketones or alcohols.

Comparing the results obtained at low temperature (130 °C, Figure 5b) with those attained with the MgAl4 sample (Figure 2a), it is possible to observe how by conducting the reaction over Cu-based catalysts in the presence of H_2, the CPO conversion is increased from 90 up to ~100% for all the samples tested. At the same time, for the 2Cu catalyst, C15 yield is enhanced up to 25% (at 130 °C), while an unchanged C10 yield was detected. Considering the nature of the products obtained, composed of aliphatic bicyclic and tricyclic ketones, it is possible to assert that this boost is attributable to a shift of the thermodynamic equilibrium derived from the hydrogenation of C=C bonds in the formed C10 and C15 aldol products, which then remain stable in these reaction conditions. By increasing the Cu content, and thus the number of the possible sites active towards hydrogenation, the progressive rapid formation of undesired cyclopentanol (CPL) is observed, limiting the condensation reaction, and consequently decreasing the production of C10 and C15. This behavior is consistent with the presented H_2-TPR profiles (Figure 4), in which the higher propensity of 10Cu towards reduction/H_2-activation is expressed in a larger formation of CPL (Yield of 23%) and a limited concentration of C15 after reaction at 130 °C (Yield of 9%). The different reducibility of the catalysts influences the outputs of the combined process in a similar way even at higher reaction temperatures. The results obtained at 150 °C (Figure 5c) show how, at constant (and total) CPO conversion, the different Cu contents influence both the distribution of the products and their nature. In this case, the

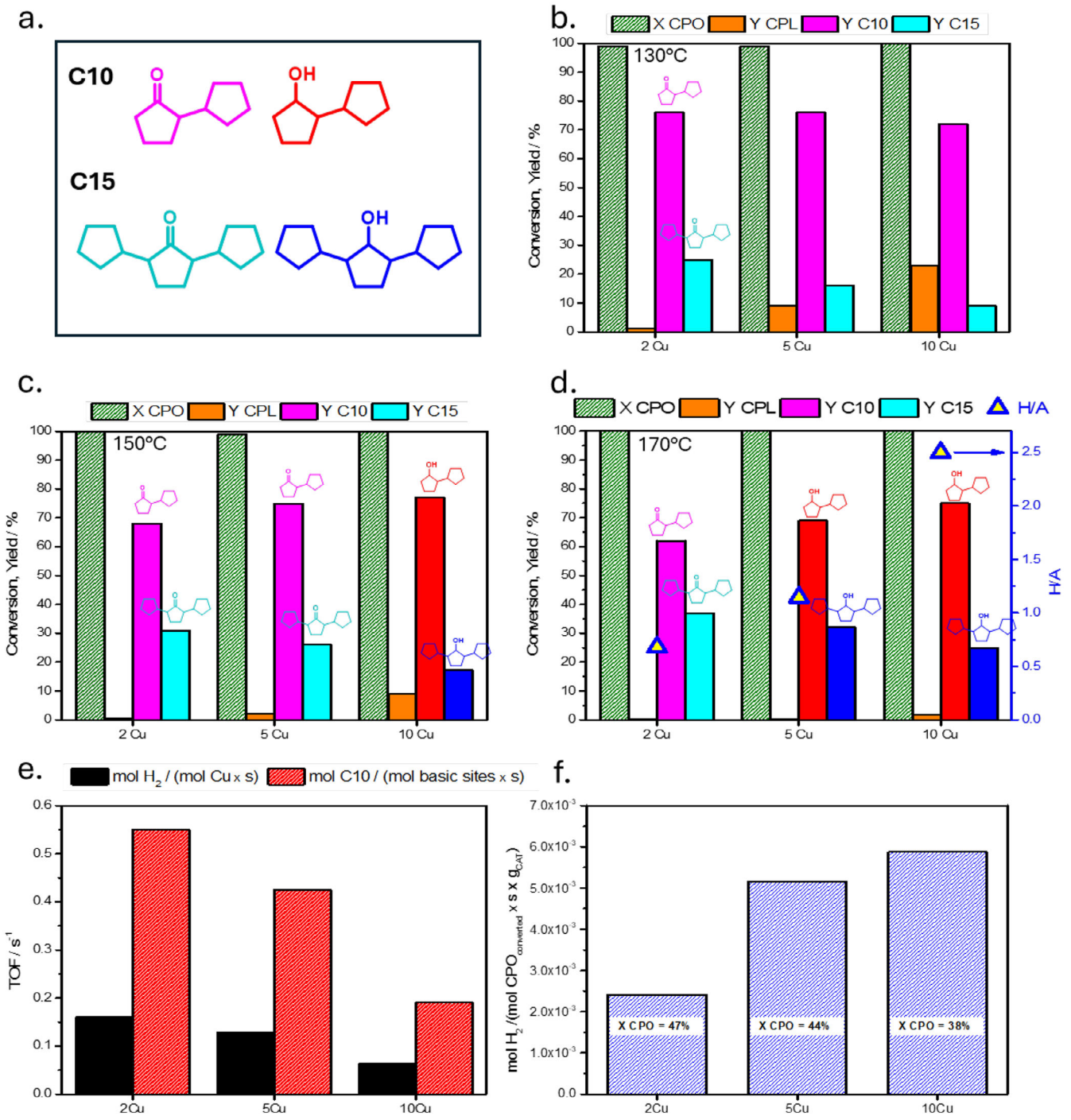

Figure 5. Activity of the Cu-based catalysts in terms of CPO conversion, cyclopentanol (CPL), and C10-15 yields at different reaction temperature: a) structures of the reaction products determined by GC-MS analyses, the different colors correspond to those of the bars showing the catalytic performances. Catalysts performance at b) 130 °C, c) 150 °C, d) 170 °C. Reaction conditions: 44 mmol of CPO, 0.5 g of CAT and 30 mL of cyclohexane, reaction time of 4 h, H_2 pressure of 1.0 MPa. Intrinsic catalytic acitivity of the catalysts: e) Turnover frequency (TOF) values of the catalysts for both hydrogenation and aldol condensation sites, f) amount of H_2 consumed per quantity of CPO converted over time as a function of the three catalysts tested. Reaction conditions: 44 mmol of CPO, 0.05 g of CAT and 30 mL of cyclohexane, reaction time of 1 h, H_2 pressure of 1.0 MPa. The amount of basic sites was extrapolated from CO_2-TPD analyses.

CPL formation is more than halved for the 10Cu (Y_{CPL} = 10%) while becoming almost negligible in the case of 5Cu and 2Cu. The lower tendency of the latter to hydrogenate the C=C bonds, leads to the highest C15 yield (31%) and to the formation of cyclic ketones after 4 h of reaction.

On the contrary, 10Cu catalyst hit a yield of 77% of the desired C10 product, forming a significantly lower amount of C15 (Y_{C15} = 17%) and exhibiting a final mixture composed only by aliphatic cyclic alcohols derived from the subsequent hydrogenation of the C=O bond of the aldol condensates. The

formation of CPL is substantially suppressed when the reaction temperature is increased to 170 °C (Figure 5d) with a yield lower than 2% for the 10Cu catalyst. Although at low Cu content the formation of ketones is still prominent with a C15 yield that reached a value of 37% for 2Cu after 4 h, both 5Cu and 10Cu samples lead to the production of an alcoholic mixture, with 10 Cu exhibiting the highest yield in bicyclic compounds ($Y_{C10} = 75\%$) indicating its superior activity in H_2 activation.

In accordance with the results obtained, it can be asserted that the tendency to form C15 products is an expression of the propensity of the catalysts to favor aldol condensation reaction over hydrogenation while, on the other hand, a consistent formation of aliphatic C10 cyclic ketone or alcohol (and CPL) likely indicates a higher hydrogenating potential of the catalyst. Starting from these premises and comparing these last results with those obtained over the Cu-based catalysts at 170 °C in an inert atmosphere (1.0 MPa of N_2, aldol condensation only, Figure 2b), a nondimensional factor which qualitatively expresses the tendency of the catalysts to favor hydrogenation over aldol condensation can be calculated (H/A, equation 5 of experimental section). As reported in Figure 5d, the obtained values show a trend that almost proportionally reflects the different Cu wt % of the catalysts, going from an H/A factor of 2.5 for 10Cu, to 1.2 and 0.7 for 5Cu and 2Cu samples respectively, confirming the prominent role of the Cu content in driving products distribution and boosting the condensation–hydrogenation process.

By decreasing the amount of catalyst and reaction time it was possible to study the intrinsic activity of both Cu and surface basic sites at 170 °C. In these conditions, it was in fact possible to limit the condensation–hydrogenation process towards the formation of only the first C10 condensation product (2-cyclopentylidene-cyclopentanone) and its subsequent hydrogenation product (2-cyclopentyl-cyclopentanone).

The turnover frequency (TOF) values of the two distinct types of sites as a function of the catalyst used are reported in Figure 5e. As expected, the TOF values calculated on the activity of the surface basic sites (red bars) increase as the amount of Cu in catalyst formulation decreases (and the concentration of surface basic sites increases, Figure 3b). This is in full agreement with the various catalytic results discussed and the higher tendency of 2Cu sample (TOF of 0.55 s^{-1}, calculated as mol C10/ mol basic sites) to favor aldol condensation in the conditions tested.

Similarly, the TOF values calculated for the hydrogenation reaction (expressed as H_2 consumption x mol Cu^{-1} x s^{-1}, black bars of Figure 5e) show how the intrinsic activity of the 2Cu sites towards H_2 activation is significantly higher than the others, whose TOF decreases gradually as the amount of Cu in catalyst increases. This result is not unexpected since, as widely reported in literature,[34,32,35] these ternary catalytic systems are characterized by a progressive decrease of Cu NPs size (and thus by an higher intrinsic activity) as the concentration of Cu in the precursors decreases. By correlating these results with those obtained in the different activity tests, it is possible to assert that in the proposed combined process, Cu concentration plays a predominant role in the reaction outputs compared to the intrinsic activity of the individual hydrogenation active sites. To further confirm this, Figure 5f shows the amount of H_2 consumed per quantity of CPO converted over time as a function of the three catalysts tested in the same conditions. These values clearly show how, even at lower CPO conversion, 10Cu catalyst favors the rapid hydrogenation of the substrates by an amount (in accordance with the calculated H/A ratio previously discussed) approximately 2.5 times larger than 2Cu. It can therefore be concluded that the combination between this property and the lower intrinsic activity of 10Cu catalyst towards condensation reaction, is the factor that limits an overproduction of C15 compounds and favors the subsequent hydrogenation of the formed cyclic ketones producing an alcoholic mixture rich in valuable C10 SAF precursors in short reaction time.

It is noteworthy that, in this context, also the operating H_2 pressure clearly plays a dominant role in products distribution, meaning that this variable must be carefully considered and properly tuned when other operating conditions (or catalyst nature) are significantly changed. As an example, in Figure S2, the catalytic results obtained over 10Cu at 170 °C by varying the operating H_2 pressure are reported. Halving this parameter (0.5 MPa of H_2) leads to a slight decrease of CPO conversion ($X_{CPO} = 95\%$) together with the formation of a complex mixture composed of α, β-unsaturated and aliphatic ketones. On the other hand, a H_2 pressure of 2.0 MPa greatly enhances the hydrogenation rate of the catalyst, favoring CPL formation ($Y_{CPL} = 25\%$) and the production of mainly C10 cyclic alcohol ($Y_{C10} = 65\%$). Notably, performing an ex situ prereduction step of 10Cu catalyst at 170 or 400 °C (40 mL min^{-1} of H_2 for 4 h) did not significantly affect the catalyst activity at 170 °C (H_2 pressure of 1.0 MPa, Figure S3), suggesting that the steps involved in the formation of surficial Cu^0 active sites during the process do not significantly influence reaction output in the tested conditions.

The XRD patterns of the catalysts after reaction as a function of working temperature are depicted in Figure 6. Regardless of Cu content, intense peaks belonging to a mixed Mg/Cu/O phase (as before reaction, Figure 1b) were observed especially for 5Cu and 10Cu catalysts, in accordance with their higher Cu content.

Interestingly, several peaks related to the reconstruction of the hydrotalcite structure were observed, the extent formation of which appears to be related to the reaction temperature of the process. Specifically, it is easy to notice that as the temperature increases these peaks become more intense, showing how the formation of water during the condensation–hydrogenation process favors the well-known "memory effect", typical of materials obtained from hydrotalcite-type precursors.[36] In addition to this, it is also possible to observe a possible relationship between hydrotalcite reconstruction and Cu content. Comparing the XRD patterns obtained for the spent catalysts at 170 °C, 10Cu catalyst, although showing a small peak attributable to the presence of Cu^0 (Figure 6c, starting from 150 °C), exhibits a higher stability of the oxide structure and a small extent of hydrotalcite-type phase after 4 h of reaction.

2.3. Catalyst Deactivation and Regeneration

The stability of 10Cu catalyst was assessed by testing the spent sample in a second reaction cycle. Before the activity test, the

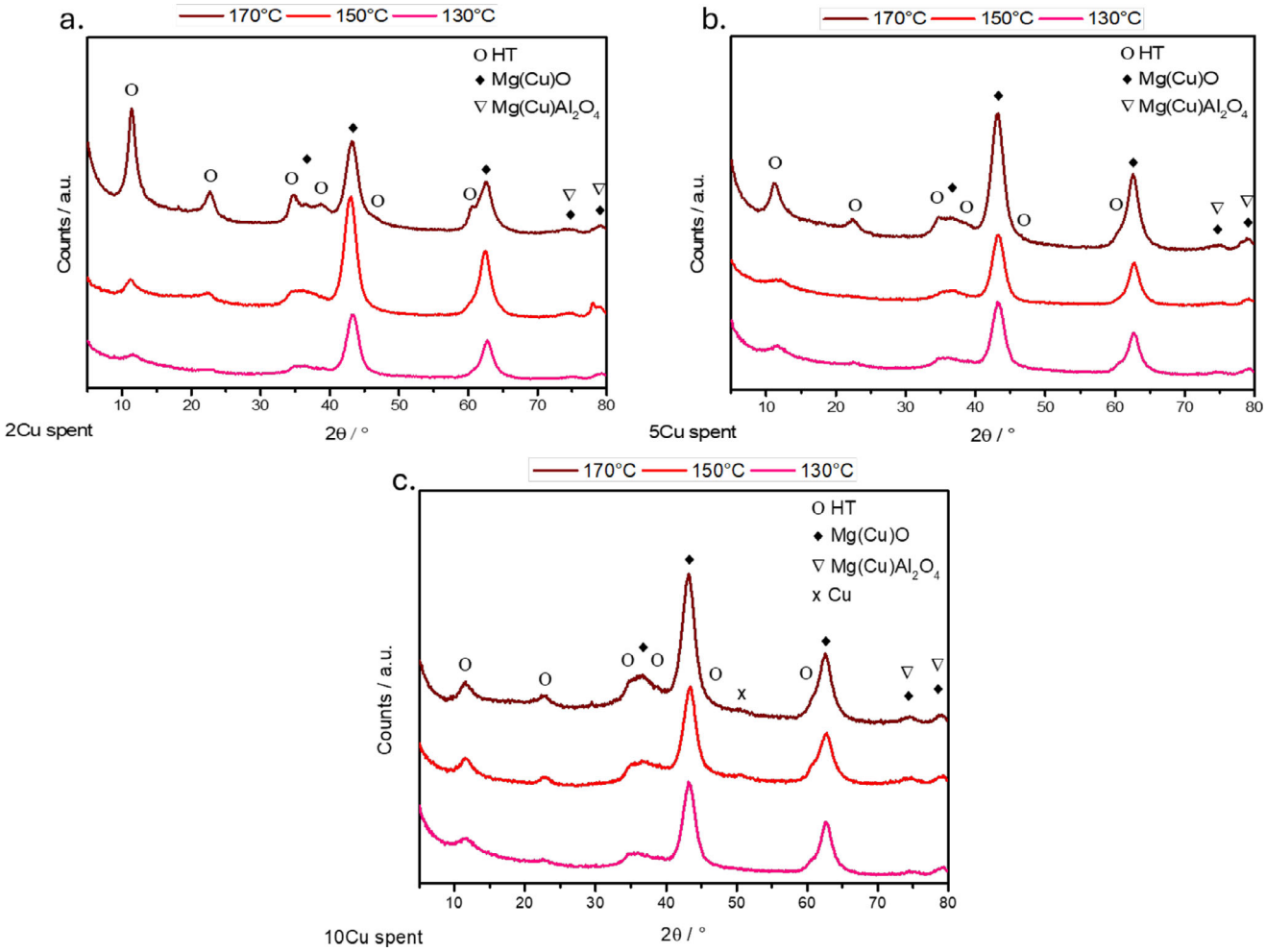

Figure 6. XRD patterns of the catalysts after 4 h of reaction as a function of operating temperature: a) 2Cu, b) 5 Cu, and c) 10Cu.

catalyst was washed with 2-propanol and dried overnight at 70 °C. Although 10Cu was still active in a second reaction cycle (Figure 7a), a significantly different distribution of the products was observed. CPO conversion was decreased to a value of 90% while CPL was formed to a high extent (Y_{CPL} = 29%). The calculated H/A factor hit a value of 25.4, 10 times folder than that observed in the first reaction cycle, evidencing the higher tendency of the catalyst to favor hydrogenation over condensation, possibly due to a loss of surface sites active in aldol reaction during the first reaction cycle. From the FT-ATR spectra of the spent catalysts at different reaction temperatures (Figure S4), the deposition of significant amounts of deactivating heavy compounds during reaction can be excluded. The calcined materials exhibit adsorption bands in the 600–1450 cm^{-1} and 1500–1650 cm^{-1} regions attributable to Mg-O vibrations and O—H bending mode respectively,[37,38] while HT and spent samples show similar spectra with characteristic bands typical of hydrotalcite-type material.[39,40] The broad band at 3540 cm^{-1} is associated with O—H stretching vibration of the metal hydroxide layer and interlayer water molecules, the latter causing also the broad bending vibration peak centered around 1640 cm^{-1}, while the band at 1360 cm^{-1} can be attributed to the vibration of carbonate species, confirming the partial reconstruction of hydrotalcite phases during reaction which is then the main cause of catalyst deactivation after first reaction cycle. To further confirm this hypothesis, the catalytic performance of 10Cu HT in the condensation–hydrogenation process was assessed. As shown in Figure S5, the 10Cu catalyst before calcination exhibit a substantial lower activity in reaction conditions, forming a mixture of products composed by unconverted CPO (X_{CPO} = 90%), CPL (Y_{CPL} = 9%) produced over Cu^0 sites generated during reaction, condensation products and aliphatic cyclic ketones (overall yields: Y_{C10} = 59% and Y_{C15} = 19%) likely formed over hydrotalcite —OH weak basic sites. Catalyst regeneration was then carried out by calcining the spent sample at 600°c for 4 h. The activity of 10Cu catalyst over five reaction/regeneration cycles is depicted in Figure 7b. In this way, it was possible to attained constant catalytic activity with only limited fluctuations of the calculated H/A factor, which slightly decreases after four reaction cycles to a value of 1.9, minimally affecting the reaction output (X_{CPO} = 100%, Y_{C10} = 69%, Y_{C15} = 31%). The SEM images of the 10Cu catalyst after five reaction cycles show the presence of a high number of metal particles (with a dimension of ≈ 25 nm) dispersed over the catalyst support, which appears to a have a rough and porous surface. It is noteworthy that the appearance of such visible metal particles was not detected over the ex

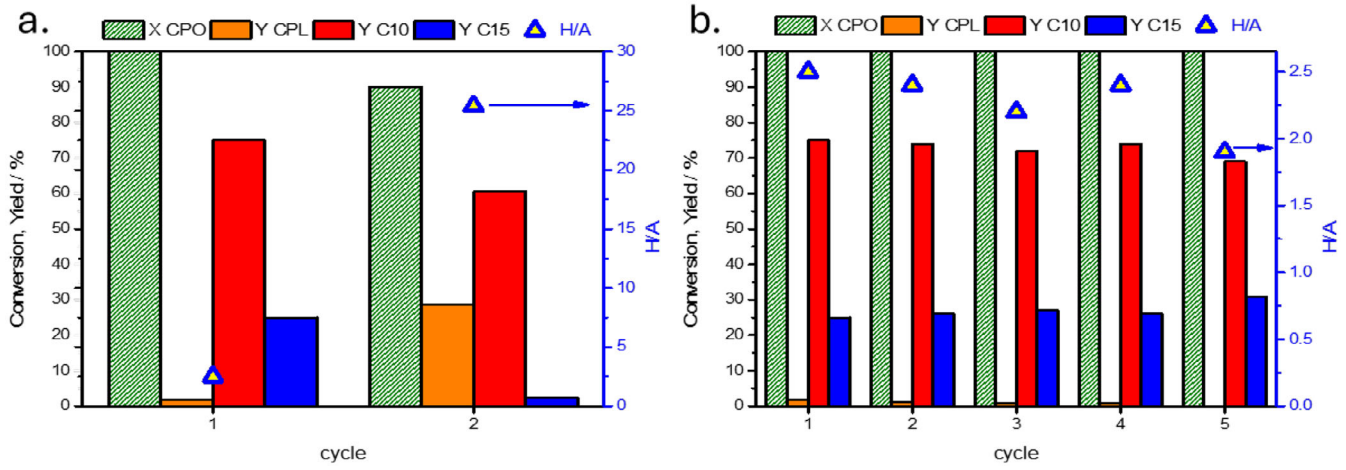

Figure 7. Activity of 10Cu catalyst at 170 °C, a) without a regeneration step and b) after consecutive calcination step at 600 °C for 4 h. C10 and C15 compounds are bicyclic and tricyclic alcohol respectively, see Figure 5a. Reaction conditions: 44 mmol of CPO, 0.5 g of CAT and 30 mL of cyclohexane, reaction time of 4 h, H_2 pressure of 1.0 MPa.

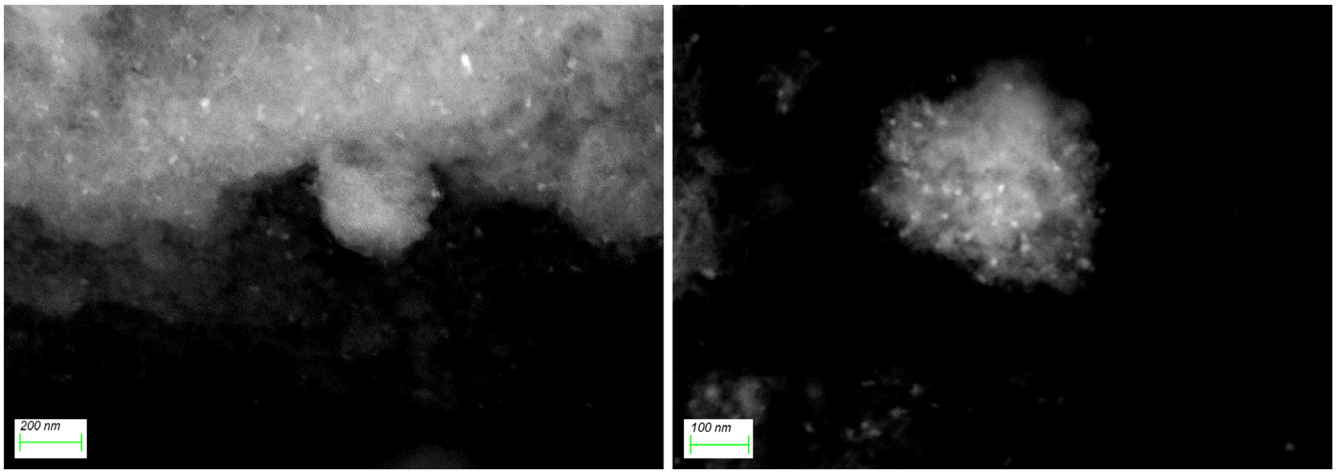

Figure 8. HR-SEM back scattered electrons images at different magnifications of 10Cu after five reaction cycles.

situ, pre-reduced 10Cu catalyst (40 mL/min of H_2, 400 °C for 4 h, Figure S6 which was active in the reaction as shown in Figure S3), likely suggesting the occurrence of sintering phenomena of the formed Cu^0 particles during the different reaction cycles. (Figure 8)

The TEM analyses of the 10Cu after the last reaction cycle confirmed the presence of highly distributed Cu^0 nanoparticles (NPs, EDS analysis in Figure S7) with a heterogeneous size distribution comprised between 1–30 nm (Figure 9a). The formed NPs show an asymmetric distribution centered around 3–4 nm with an average particle size of 7 nm (calculated over 400 particles, Figure 9b). Although a significant number of metal aggregates with a diameter beyond 10 nm was detected, roughly 65% of the total NPs exhibit a dimensional distribution <5 nm. Notably, the coexistence of Cu^0 NPs with a phase consisting of sheet-like structures typical of that of hydrotalcite[41,42] can be observed (Figure 9c and d), explaining the higher tendency of the spent catalyst in favoring hydrogenation over aldol condensation when it is used (without a regeneration step) in a subsequent reaction cycle (H/A of 25.4, Figure 7a)

3. Conclusions

CPO can be efficiently processed in a one-pot aldol condensation–hydrogenation reaction to obtain valuable and partially refined C10–15 compounds with high potential as high-energy density and low-freezing point SAF precursors. Cu-based bifunctional catalysts obtained from cheap hydrotalcite-type formulations exhibited high activity in the reaction, combining strong basic surface sites active in aldol condensation and well dispersed Cu^0 NPs which favor C=C and C=O prompt hydrogenation in mild conditions. In addition to favoring the formation of cyclic aliphatic alcohols or ketones, the presence of H_2 boosts catalytic performance, and synergically with catalyst Cu content, drives the distribution of the products favoring the formation of more desirable C10 compounds. The results obtained in both aldol condensation and combined condensation–hydrogenation process are highly competitive with those present in the literature (Table S1). Moreover, the recyclability tests performed on 10 Cu catalyst demonstrated how after a simple thermal treatment, it is possible to regen-

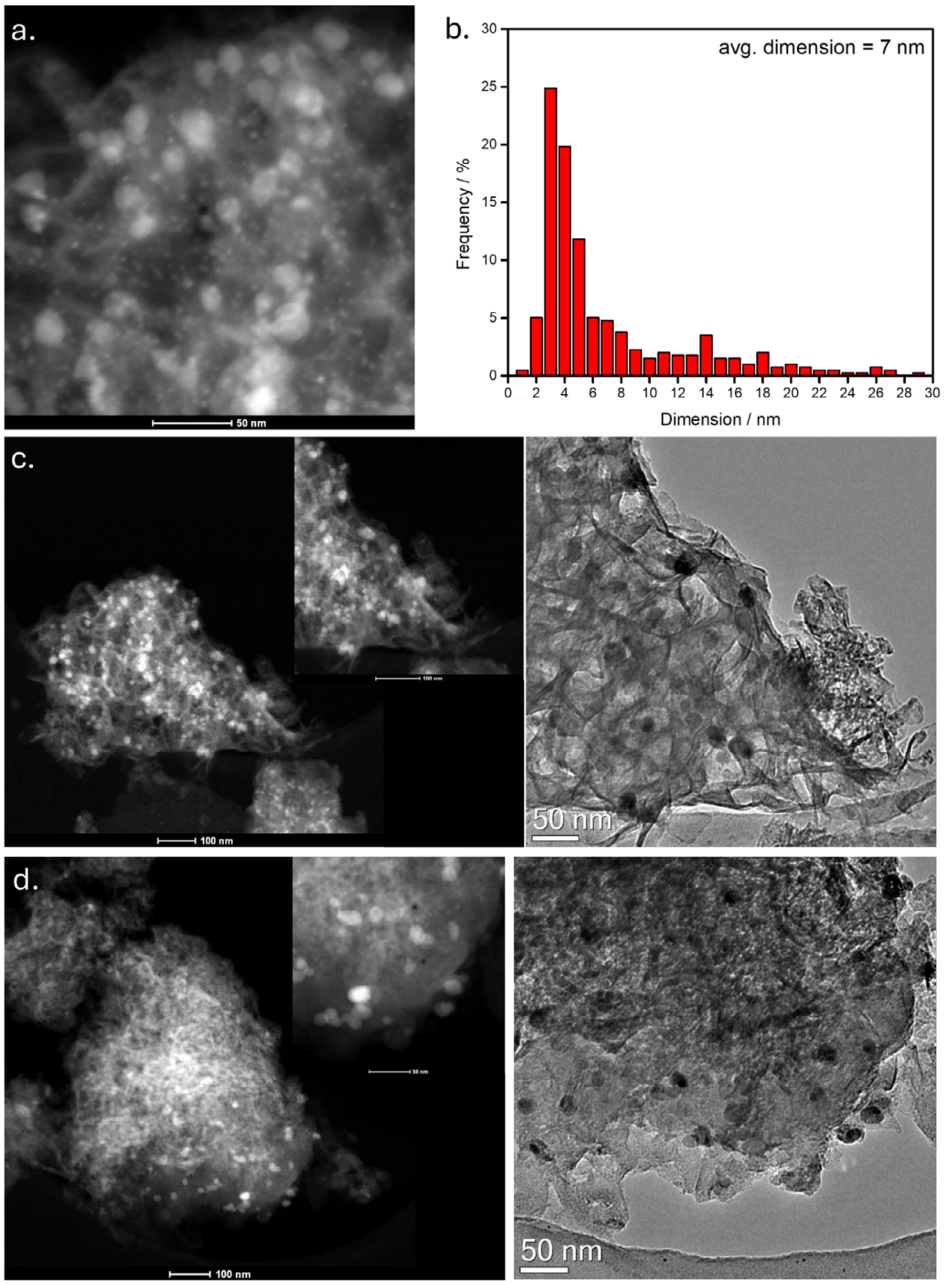

Figure 9. a) STEM-HAADF image highlighting the presence of highly dispersed small Cu^0 nanoparticles, b) NPs particle size distribution measured over 400 particles (calculated average dimension of 7 nm). c and d) STEM-HAADF and corresponding HR-TEM images of 10Cu catalyst after five reaction cycles.

erate the catalyst which, without any prereduction step, show stable performance in multiple reaction/regeneration cycles.

4. Experimental Section

4.1. Catalyst Synthesis

The hydrotalcite-type precursors with a $(Cu + Mg)^{2+}/Al^{3+}$ molar ratio of 4 and a Cu content of 0, 2, 5, 10 wt % were synthesized through coprecipitation. $Cu(NO_3)_2 \cdot 2.5H_2O$, $Mg(NO_3)_2 \cdot 6H_2O$ and $Al(NO_3)_3 \cdot 9H_2O$ were dissolved in deionized water and this solution (1 M) was added dropwise to a Na_2CO_3 solution (2 M) at 60 °C, maintaining a constant pH value of 10.0 ± 0.2 by dosing a NaOH solution (3 M). The obtained suspension was stirred for 60 min at 60 °C, filtered and washed with deionized hot water until minimum Na^+ content. The solid was then dried ad 70 °C overnight and calcined at 600 °C for 6 h (heating rate of 10 °C min^{-1}). In the tests conducted with preactivated catalysts, the calcined material (0.5 g) undergoes to an ex situ reduction in a continuous tubular isothermal reactor at 170 or 400 °C for 4 h feeding 40 mL/min of pure H_2. The acronyms for the Cu/Mg/Al/O synthesized catalysts with a Cu content of 0, 2, 5, and 10 wt % are MgAl4, 2Cu, 5Cu, and 10Cu, respectively.

4.2. Catalyst Characterization

Porosity data and surface areas of the catalysts were determined by N_2 adsorption/desorption at −196 °C by a Micromeritics ASAP 2020 instrument. 0.150 g of the samples were pretreated under vacuum at

150 °C for 1 h, pore size distribution was calculated through Barret–Joyner–Halenda (BJH) analysis method and the specific surface area calculated using the Braunauer–Emmet–Teller (BET) multiple-point method. XRD powder analyses were carried out on a Rigaku Miniflex 600 diffractometer equipped with a copper anode. The samples were investigated in a 2Θ range of 5°–80° using a step size of 0.05° and a scan step time of 15.25 s. H_2-TPR and CO_2-TPD experiments were performed using an Autochem II system (Micromeritics) equipped with a TCD. The reduction profiles were carried out after the pretreatment of the sample (0.150 g) at 500 °C for 60 min (30 mL min^{-1} of He). The reduction was carried out using a mixture of 5% H_2/Ar (30 mL min^{-1}) by increasing the temperature of the sample from 50 to 900 °C (10 °C min^{-1}). CO_2 desorption experiments were conducted by pre-reducing the catalysts (5% H_2/Ar, 30 mL min-1) at 500 °C (10 °C min^{-1}) for 60 min and exposing the samples to a 10% CO_2/Ar flow (30 mL min^{-1}) at 50 °C for 120 min. After flushing the samples with He at this temperature, the catalysts were heated up to 900 °C (10 °C min^{-1}). The desorbed amount of CO_2 was normalized over both the mass and the specific surface area of the different catalysts. The IR spectra of the catalysts before and after reaction were acquired in attenuated total reflectance (ATR) over the 600–4000 cm^{-1} range using a Thermo Scientific Nicolet iS10 Smart iTR equipped with a Smart OMNI transmission instrument. HR-SEM images were collected with a Carl Zeiss microscope (mod. Gemini 360) working in the high vacuum mode and with an acceleration voltage equal to 15kV: This value was chosen because, according to the manufacturer specifications, it allows to reach the best resolution. To better contrast metallic particles against the support, the external back scattered detector was always used. High-resolution transmission electron microscopy (HR-TEM) measurements were carried out using a TEM/STEM FEI TECNAI F20 microscope coupled with an energy-dispersive spectroscopy analyzer (EDS). Powder samples were dispersed in ethanol under ultrasonic conditions for 30 min. The obtained suspension was deposited on an Au grid with lacey multifoil carbon film and dried at 100 °C before measurements.

4.3. Catalytic Activity

The activity tests were carried out in a 100 mL stainless steel autoclave (Amar instrument) equipped with mechanical stirring. In a typical test, 44 mmol of CPO, 0.5 g of calcined catalyst and 30 mL of cyclohexane were added into the reactor. Before reaction, and depending on the test, pressurized H_2 or N_2 was flushed into the system several times to remove air. The mixture was then heated to the target temperature (130, 150 or 170 °C) under N_2 or H_2 pressure (1.0 MPa) and maintained for 4 h in these conditions. If not mentioned, the catalysts were used without any prereduction step. The reaction mixture was quantitatively analyzed using decane as internal standard in a GC Autosystem XL (Perkin Elmer) equipped with a DB-5 column and a FID detector. The structures of the reaction products were assigned using a Perkin Elmer Clarus 600 GC-MS system. The catalytic activity of the samples was evaluated using the following equations.

$$\text{Cyclopentanone conversion}\ (\text{XCPO}) = \frac{(\text{mol CPO t0} - \text{mol CPO})}{\text{mol CPO t0}} \times 100$$

$$\text{C10 Yield}\ (\text{YC10}) = \frac{2\,\text{mol C10}}{\text{mol CPO t0}} \times 100 \quad (1)$$

$$\text{C10 Selectivity (SC10)} = \frac{2\,\text{mol C10}}{(\text{CPO t0} - \text{mol CPO})} \times 100$$

$$\text{C15 Yield (YC15)} = \frac{3\,\text{mol C15}}{\text{mol CPO t0}} \times 100 \quad (2)$$

$$\text{C15 Selectivity (SC15)} = \frac{3\,\text{mol C15}}{(\text{CPO t0} - \text{mol CPO})} \times 100 \quad (3)$$

$$\text{C balance} = [\text{mol CPO t0} - (\text{mol CPO} + 2\,\text{mol C10} + 3\ \text{mol C15})] \times 100 \quad (4)$$

C balance is not reported in the different figures but always corresponded to 100 ± 2%.

Qualitative hydrogenation/aldol condensation potential factor:

$$\text{H/A} = \left(\frac{\text{SC15}}{\text{SC10}}\right)_{\text{in}N_2} / \left(\frac{\text{SC10}}{\text{SC15}}\right)_{\text{in}\,H_2} \quad (5)$$

in which "in N_2" and "in H_2" refer to the reaction atmosphere in which the process was carried out at the same temperature over the same catalyst (pressure of 1.0 MPa).

$$\text{TOF}_{\text{hydrogenation}} = \frac{\text{mol}\,H_2\ \text{consumed}}{\text{mol Cu} \bullet \text{s}} \quad (6)$$

$$\text{TOF}_{\text{condensation}} = \frac{\text{mol C10 produced}}{\text{mol basic sites} \bullet \text{s}} \times \text{basic sites extrapolated from } CO_2 - \text{TPD} \quad (7)$$

Acknowledgments

PON Ricerca e Innovazione 2014–2020 azione IV.6 (BR119), DM 10 agosto 2021 numero 1062 is acknowledged for the research grant of NS, and the financial support.

Open access publishing facilitated by Universita degli Studi dell'Insubria, as part of the Wiley - CRUI-CARE agreement.

Conflict of Interests

The authors declare no conflict of interest.

Data Availability Statement

The data that support the findings of this study are available from the corresponding author upon reasonable request.

Keywords: Biofuels · Condensation · Copper-hydrotalcite · Heterogeneous catalysis · Supported catalyst

[1] A. A. Longati, G. Batista, A. J. Gonçalves Cruz, *Curr. Opin. Green Sustain. Chem.* **2020**, *26*, 100400.
[2] A. Sonthalia, N. Kumar, *J. Energy Inst.* **2019**, *92*, 1.
[3] N. Schiaroli, M. Volanti, A. Crimaldi, F. Passarini, A. Vaccari, G. Fornasari, S. Copelli, F. Florit, C. Lucarelli, *Energy Fuels* **2021**, *35*, 4224.
[4] N. Schiaroli, M. Battisti, P. Benito, G. Fornasari, A. G. di Gisi, C. Lucarelli, A. Vaccari, *Catalysts* **2022**, *12*, 109.
[5] N. Schiaroli, C. Lucarelli, M. C. Iapalucci, G. Fornasari, A. Crimaldi, A. Vaccari, *Catalysts* **2020**, *10*, 1345.
[6] P. H. Ho, G. Sanghez de Luna, N. Schiaroli, A. Natoli, F. Ospitali, M. Battisti, F. di Renzo, C. Lucarelli, A. Vaccari, G. Fornasari, P. Benito, *Ind. Eng. Chem. Res.* **2022**, *61*, 10511.

[7] P. Tarifa, N. Schiaroli, P. H. Ho, F. Cañaza, F. Ospitali, G. Sanghez de Luna, C. Lucarelli, G. Fornasari, A. Vaccari, A. Monzon, P. Benito, *Catal. Today* **2022**, *383*, 74.
[8] R. Thomson, P. Kwong, E. Ahmad, K. D. P. Nigam, *Int. J. Hydrog. Energy* **2020**, *45*, 21087.
[9] J. R. Melendez, B. Mátyás, S. Hena, D. A. Lowy, A. E. Solous, *Renew. Sustain. Energy Rev.* **2022**, *160*, 112260.
[10] A. T. Hoang, H. C. Ong, I. M. Rizwanul Fattah, C. T. Chong, C. K. Cheng, R. Sakthivel, Y. Sik Ok, *Fuel Process. Technol.* **2021**, *223*, 106997.
[11] S. Albonetti, E. Boanini, I. Jiménez-Morales, C. Lucarelli, M. Mella, C. Molinari, A. Vaccari, *RSD Adv.* **2016**, *6*, 48962.
[12] C. Lucarelli, G. Pavarelli, C. Molinari, S. Albonetti, W. Mista, D. Di Domenico, A. Vaccari, *Int. J. Hydrog. Energy* **2014**, *39*, 1336.
[13] U. S. Department of Energy, Office of Energy efficiency & renewable energy, "Sustainable Aviation Fuel – Review of technical pathways", can be found under https://www.energy.gov/eere/bioenergy/articles/sustainable-aviation-fuel-review-technical-pathways-report, **2020** (accessed: July 2024).
[14] K. Yan, G. Wu, T. Lafleur, C. Jarvis, *Renew. Sustain. Energy Rev.* **2014**, *38*, 663.
[15] L. Grazia, T. Della Rosa, D. Bonincontro, T. Tabanelli, N. Schiaroli, F. Cavani, C. Lucarelli, S. Albonetti, *Catal. Today* **2023**, *420*, 114036.
[16] J. He, Q. Qiang, S. Liu, K. Song, X. Zhou, J. Guo, B. Zhang, C. Li, *Fuel* **2022**, *306*, 121765.
[17] J. P. Lange, *Catal. Today* **2024**, *435*, 114726.
[18] X. Liao, H. Zhao, R. Liu, H. Luo, Y. Lv, P. Liu, *J. Catal.* **2024**, *436*, 115603.
[19] J. Yang, N. Li, G. Li, W. Wang, A. Wang, X. Wang, Y. Cong, T. Zhang, *Chem. Commun.* **2014**, *50*, 2572.
[20] D. T. Ngo, T. Sooknoi, D. E. Resasco, *Appl. Catal. B* **2018**, *237*, 835.
[21] D. Liang, G. Li, Y. Liu, J. Wu, X. Zhang, *Catal. Commun.* **2016**, *81*, 33.
[22] S. Shao, W. Dong, X. Li, H. Zhang, Y. R. Xiao, *J. Clean. Prod.* **2020**, *250*, 119459.
[23] Q. Deng, G. Nie, L. Pan, J. J. Zou, X. Zhang, L. Wang, *Green Chem.* **2015**, *17*, 4473.
[24] W. Wang, X. Zhang, Z. Jiang, Y. Cui, Q. Kang, X. Zhao, Q. Zhang, L. Ma, *Fuel* **2022**, *321*, 124114.
[25] Q. Deng, H. Peng, Z. Yang, T. Wang, J. Wang, Z. Zeng, S. Dai, *Appl. Catal. B* **2023**, *337*, 122982.
[26] T. Li, J. Su, L. Yin, X. Zhang, C. Wang, X. Li, J. Zhang, K. Wang, *Green Chem.* **2024**, *26*, 1910.
[27] S. Kannan, A. Dubey, H. Knozinger, *J. Catal.* **2005**, *231*, 381.
[28] J. J. Bravo-Suárez, B. Subramaniam, R. V. Chaudhari, *J. Phys. Chem. C* **2012**, *116*, 18207.
[29] V. K. Díez, C. A. Ferretti, P. A. Torresi, C. R. Apesteguía, J. I. Di Cosimo, *Catal. Today* **2011**, *173*, 21.
[30] C. Lucarelli, C. Molinari, R. Faure, G. Fornasari, D. Gary, N. Schiaroli, A. Vaccari, *Appl. Clay Sci.* **2018**, *155*, 103.
[31] B. K. Kwak, D. S. Park, Y. S. Yun, J. Yi, *Catal. Commun.* **2012**, *24*, 90.
[32] H. Liu, W. Huang, Z. Yu, X. Wang, Y. Jia, M. Huang, H. Yang, R. Li, Q. Wei, Y. Zhou, *Mol. Catal.* **2024**, *558*, 114002.
[33] T. Kondratowicz, O. Horký, S. Slang, L. Dubnová, M. Gajewska, L. Chmielarz, L. Čapek, *Nanoscale Adv.* **2023**, *5*, 3063.
[34] T. B. Jayesh, K. Itika, G. V. Ramesh Babu, K. S. Rama Rao, R. S. Keri, A. H. Jadhav, B. M. Nagaraja, *Catal. Commun.* **2018**, *106*, 73.
[35] H. Liu, Y. Jiang, H. Zhao, Z. Hou, *J. Ind. Eng. Chem.* **2021**, *102*, 251.
[36] A. Vaccari, *Catal. Today* **1998**, *41*, 53.
[37] N. Siddqui, B. Sarkar, C. Pendem, R. Khatun, L. N. S. Konthala, T. Sasaki, A. Bordoloi, R. Bal, *Catal. Sci. Technol.* **2017**, *7*, 2828.
[38] E. Aliyari, M. Alvand, F. Shemirani, *RSC Adv.* **2016**, *6*, 64193.
[39] D. Kwon, J. Y. Kang, S. An, I. Yang, J. C. Jung, *J. Energy Chem.* **2020**, *46*, 229.
[40] M. Bouraada, M. S. Ouali, L. C. de Ménorval, *J. Saudi Chem. Soc.* **2016**, *20*, 397.
[41] S. Nishimura, A. Takagaki, K. Ebitani, *Green Chem.* **2013**, *15*, 2026.
[42] K. Simeonidis, E. Kaprara, P. Rivera-Gil, R. Xu, F. J. Teran, E. Kokkinos, A. Mitropoulos, N. Maniotis, L. Balcells, *Nanomaterials* **2021**, *11*, 1796.

Manuscript received: October 10, 2024
Accepted manuscript online: November 03, 2024
Version of record online: ■■, ■■